NANO LETTERS

Letter

pubs.acs.org/NanoLett

Tunable Assembly of Heterogeneously Charged Colloids

Emanuela Bianchi,*[,†] Christos N. Likos,[‡] and Gerhard Kahl[†]

[†]Institut für Theoretische Physik and Center for Computational Materials Science (CMS), Technische Universität Wien, Wiedner Hauptstraße 8-10, A-1040 Wien, Austria

[‡]Faculty of Physics, University of Vienna, Boltzmanngasse 5, A-1090 Vienna, Austria

Supporting Information

ABSTRACT: The self-assembly of colloidal particles is a route to designed materials production that combines high flexibility, cost effectiveness, and the opportunity to create ordered structures at length scales ranging from nano- to micrometers. For many practical applications in electronics, photovoltaics, and biomimetic material synthesis, ordered mono- and bilayers are often needed. Here we present a novel and simple way to tune via external parameters the ordering of heterogeneously charged colloids into quasi two-dimensional structures. Depending on the charges of the underlying substrate and of the particles, a rich and versatile assembly scenario takes place, resulting from the complex interplay between directional attractive and repulsive particle−particle and particle−substrate interactions. Upon subtle variations of the relative charge of the system components, emerging via pH modification, reversible changes either from extended aggregates to a monomeric phase or from triangular to square domains are observed.

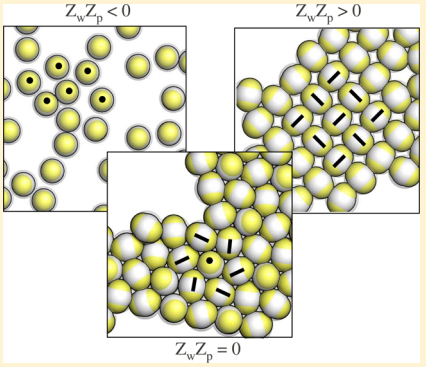

KEYWORDS: *Inverse patchy colloids, heterogeneously charged particles, self-assembly, charged substrates, quasi two-dimensional confinement*

Low-dimensional systems, built-up by units of specific, well-defined particle arrangements, are of paramount relevance in the wide field of functional materials with applications as antireflection coatings, biosensors, data-storage devices, lithography masks, catalysts, or optical and photovoltaic devices.[1−4] The quality and the reproducibility of the desired properties of these materials strongly depend on how accurately one can steer their production process, which often consists of tailored self-organization mechanisms, possibly supported by the presence of a substrate. The realization of mono- and bilayer assemblies on surfaces is governed by a delicate balance between a multitude of factors, including the properties of the assembling units, the physical and/or chemical characteristics of the underlying, smooth, or patterned surface, and the relative strengths of the interparticle and particle−substrate interactions.

At the atomic level, the production processes of a wide range of surface structures[5−7] are defined and delimited by many phenomena, such as the electronic properties of the entities involved (i.e., atoms and molecules), hydrogen and covalent bonding, or dipolar coupling. At the colloidal level, the possibilities of rational materials design are enhanced by the ability to tune, in a controlled fashion, the interactions between the entities involved as well as the size of the self-assembling units. The colloidal size can be chosen from the nanometer up to the micrometer scale, thus introducing a length scale comparable to the wavelength of light in the self-assembled products, which can acquire interesting photonic properties.[8] The interparticle interactions themselves can be designed during the particle synthesis and further modified during assembly, offering a tremendous variety of functional materials. Control over the interparticle interactions can be achieved by varying the particle architecture or the properties of the microscopic solvent in which colloidal particles are dispersed,[9] while in multicomponent colloidal systems, the variety of self-assembly scenarios can be further broadened by the disparity in the properties of the different species.[10−12] As a consequence of their larger size, colloids are relatively susceptible to the influence of external fields. In quasi-two-dimensional geometries, field-directed assembly of colloids has resulted in, for instance, self-healing membranes[13] and perfectly hexagonal planar domains.[14−16] By exposing multicomponent dispersions to external fields and/or nematic solvents, more exotic structures with triangular-packed, square-packed, Kagome, and honeycomb arrays can be assembled.[17−19] Additionally, light[20,21] and magnetic[22] fields that exhibit intensity variations on the length scale of individual colloids can be used to shape the energy landscape, thus steering the assembly into aperiodic or quasi-crystalline structures. Local order can also be imposed by patterned substrates.[23]

Another route to produce ordered colloidal arrays rests on anisotropy-driven self-assembly. By manipulating the shape and/or the surface properties of the colloids, interparticle interactions can indeed be designed to be direction-dependent. Convex, anisometric particles display interesting phases when

Received: March 12, 2014
Revised: May 15, 2014
Published: May 19, 2014

   dx.doi.org/10.1021/nl500934v | *Nano Lett.* 2014, 14, 3412−3418

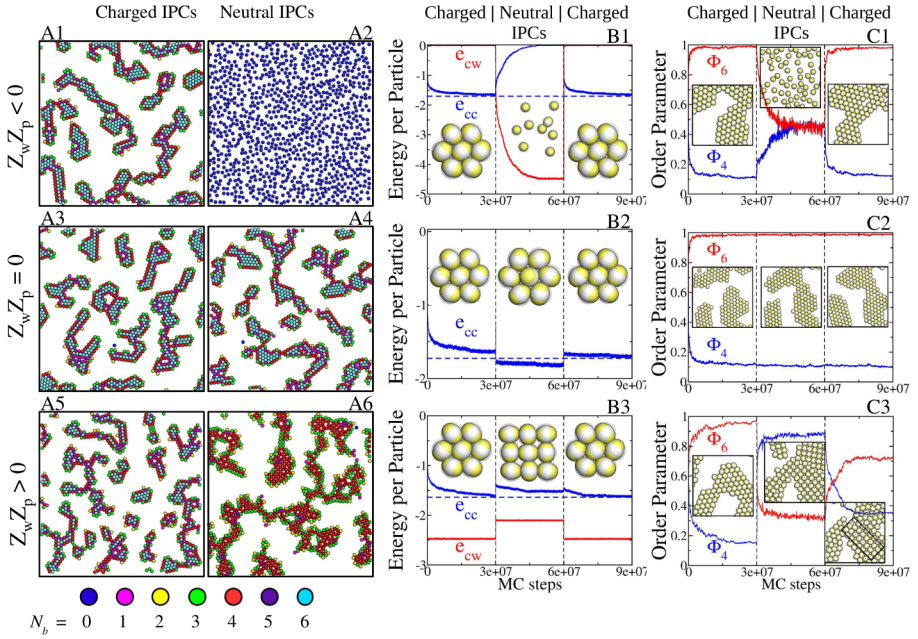

Figure 1. Panels A1−A6: typical simulation snapshots of the two investigated types of IPCs—i.e., overall charged (left column) and neutral (right column) particles, as labeled—under tight confinement between two parallel walls; the top wall is always neutral, while the bottom wall can be either neutral (panels in the central row, labeled with $Z_wZ_p = 0$) or charged (panels in the top and bottom rows, labeled with $Z_wZ_p < 0$ and $Z_wZ_p > 0$, respectively). Particles are colored according to the number of bonded interactions: two particles are defined as bonded when their pair interaction energy is less than zero; the corresponding color code is displayed at the bottom of the A-panels. Panels B1−B3 and C1−C3: the effects of a sudden change in the particle charge, showing the energy per particle (left column) and the two-dimensional order parameters Φ_4 and Φ_6 (right column) as functions of MC steps; in both columns, panels in the central row refer to the case $Z_wZ_p = 0$, while the top and the bottom rows show the results of the case $Z_wZ_p < 0$ and $Z_wZ_p > 0$, respectively. Each panel is divided into three sections by vertical dashed lines indicating the switch (i) from charged to neutral particles and (ii) from neutral to charged particles, as labeled. In each distinct section, isolated units (panels B1−B3) or significant parts (panels C1−C3) of the corresponding structures are reported as insets. The rectangle highlighted inside the snapshot of charged IPCs when $Z_wZ_p > 0$ (C3, third section) delimits the region where particles have a square arrangement, in contrast to the triangular arrangement that characterizes the overwhelming part of the system. In panels B1−B3, the particle−particle e_{cc} and the particle−wall e_{cw} energies are reported separately, as labeled. In panels C1−C3, the order parameters Φ_4 and Φ_6 are shown, calculated according to eq 1.

confined to quasi two-dimensional geometries: depending on the colloidal shape a variety of superstructures has been reported, such as cubic monolayers, fluid-like membranes that are comparable to those of lipid bilayers, and monolayers of octapods with a rich phase behavior.[24−26] Anisotropic interactions can also originate from heterogeneous particle surfaces, featured in colloids commonly referred to as patchy particles.[27,28] Patchy systems have been recently observed to self-organize into an planar Kagome lattice with well-defined structural properties.[29] The great potentialities offered by patchy systems are furthermore enhanced if the patches are sensitive to an external drive. Under the influence of electric or magnetic fields, formation of chains, staggered chains, or close and loosely packed two-dimensional crystals are obtained, depending on the field intensity and/or frequency.[30−34]

Here we propose a novel, yet unexplored route to steer in a reliable and reversible manner the self-assembly of colloidal particles in quasi two-dimensional systems. This control is achieved via moderate modifications of a few, experimentally accessible external parameters. We consider colloidal particles with heterogeneously charged surfaces, so-called inverse patchy colloids (IPCs),[35] with two charged, broad polar caps (patch opening angle $\gamma = 60°$) and an oppositely charged equatorial region; a schematic IPC is represented in Figure 1 of the Supporting Information. Depending on the charge balance between the different surface regions, IPCs can be overall either neutral or charged. An aqueous solution of IPCs is confined between two horizontal, parallel planes either under tight or loose confinement conditions. For the theoretical modeling of the interparticle and particle−wall interactions, we employ a microscopic-based, coarse-graining procedure developed in refs 35 and 36. The parameters of such potentials and the features of the confinement are specified in Section I of the Supporting Information together with the details about the Monte Carlo simulations used to study the aggregation processes of the selected systems. Experimental systems that feature inhomogeneously charged surfaces are diverse: they include, e.g., PbS−Au_4 nanostructures and PbS−Au_n nanocubes,[37] the recently synthesized spotted vesicles,[38] viral capsids, and virus-like nanoparticles.[39,40] In the latter case, the overall particle charge can be controlled via pH modifications,[39] allowing for a tuning of both their propensity to act as assembly sites for viral capsids and their functionality as building blocks for two-dimensional self-assembly into ordered structures.[39,41]

The variety of the identified assembly scenarios is summarized in panels A1−A6 of Figure 1 for systems under tight confinement, and it demonstrates that the self-organization of IPCs can be triggered by controlling the competition between the attractive and repulsive interactions involved. Changes in the vertical direction correspond to a change of the wall charge Z_w, whereas those in the horizontal direction pertain to a modification of the overall particle charge $Z_{tot} = Z_c + 2Z_p$, where Z_c is the charge of the bare colloid (without the patches) and Z_p is the charge of a patch. Mere inspection of Figure 1 provides evidence of a broad variety of self-assembled configurations: the scenarios range from a fluid-

dx.doi.org/10.1021/nl500934v | Nano Lett. 2014, 14, 3412−3418

like, disordered phase of isolated particles to various extended structures composed of linked domains that feature a multitude of internal, both translational and orientational, types of order. Such particle networks characterized by short-range order and long-range disorder have been referred to as microcrystalline gels in ref 36. There, narrower patches of angular extent $\gamma = 30°$ and $\gamma = 45°$ have been considered, resulting, in many occasions, into disordered structures or in local hexagonal, grain-like ordering. Here, the broad patch angle $\gamma = 60°$ brings forward a wealth of novel features: the local arrangement is always ordered, but the type of ordering varies from grain-like to flower-like to square patterns. Moreover, we demonstrate that one can reversibly switch between the different types of local ordering via modification of the particle− or wall−properties, the switching occurring either in a direct way or through a pathway passing via a single, disordered structure.

In view of the rich aggregation behavior, it is appropriate to start from the simplest situation, where overall neutral particles are adsorbed on a substrate that carries a charge such that $Z_wZ_p < 0$ (panel A2). The attraction between one of the patches and the substrate in combination with the mutual repulsion between the equatorial regions of neighboring particles induces a disordered, fluid-like arrangement of isolated ICPs with their symmetry axes oriented perpendicular to the substrate (panel B1 of Figure 1, middle).

Switching off the wall charge allows the particles to optimize their mutual arrangement and assemble into a gel-like network of crystalline domains with a characteristic internal structure (panel A4): while spatially arranged in a simple triangular lattice, particles self-organize into a complex orientational pattern. The spatial and orientational features of the aggregates guarantee that the energy of the configuration is minimized via an optimal bonding between the polar and the equatorial regions of neighboring particles. By pure visual inspection it is possible to identify hexagonally ordered domains where rings of six particles with horizontally oriented symmetry axes host in their center a single particle in an *up-right* position. Triangular domains with such a *flower*-like bonding pattern are referred to as "f-triangles" (panel B2 of Figure 1, middle).

When the wall charge has the same sign of the patch charge, i.e., $Z_wZ_p > 0$, polar patches are repelled by the substrate and IPCs with their axes parallel to the walls are energetically favored, meaning that the most advantageous particle orientation is not compatible with the f-triangle structure. Due to the competition between the attractive and repulsive components of the interparticle and particle−substrate interactions, T-shape (i.e., mutually orthogonal) configurations of neighboring particles emerge so that the horizontal particle orientation and the formation of interparticle bonds are both guaranteed, leading on a larger scale to a square lattice (panel B3 of Figure 1, middle). This dramatic structural change between the triangular and the square scenario is induced by a relatively small wall charge, namely, $|Z_w| \approx 0.05|Z_p|$.

The corresponding cases for overall charged particles (with $Z_{tot}Z_c > 0$) are summarized in panels A1, A3, and A5 for the three choices of the wall charge. Irrespective of Z_w, the system forms a microcrystalline gel where the particles arrange in triangular domains, whose size is slightly dependent on the charge of the substrate: ordered regions become smaller as we change Z_wZ_p from a negative to a positive value. In all three cases, the orientational vectors of the particles are predominantly oriented along the horizontal direction and form an angle of approximately 60° with the symmetry axes of the neighboring particles. Triangular aggregates with such a *grain*-like bonding pattern are referred to as "g-triangles" (panels B1/B2/B3 of Figure 1, both sides). Via simple reasoning it is possible to understand why the formation of the g-triangles is not affected by the charge of the substrate: (i) when $Z_wZ_p = 0$, the IPCs self-organize in such a way that the interparticle bonds are saturated in an optimum way; (ii) for $Z_wZ_p < 0$, the patch−wall attraction is overruled by the interparticle bonding mechanism behind the grain-like pattern and, since the equatorial regions carry charges of the same sign as the wall charge, the entire particle cluster is repelled from the substrate such that it "floats" above the bottom wall; (iii) in the case $Z_wZ_p > 0$, the interparticle bonds are again saturated by an essentially horizontal grain-like particle arrangement, but in contrast to case (ii) the attraction between the equatorial regions of the particles and the substrate leads to the adsorption of the domains to the bottom wall. Such an adsorption leads to a reduced rotational mobility of the particles and is thus mainly responsible for smaller domains as compared to cases (i) and (ii) where the distance between the domains and the substrate is considerably larger. A more detailed analysis of the translational and orientational order characterizing the different self-assembled structures under tight confinement is reported in the Supporting Information.

The characteristic and pronounced differences in the self-organization scenarios of neutral and charged IPCs for a fixed wall charge call for a deeper investigation aimed to understand if and how the morphology of the aggregates can be reversibly tuned. To this end, we simulate a charging−decharging process of the particles as it can be realized in an experimental system by modifying, for instance, the pH value of the solvent.[39] On changing the pH of a solution, the association/dissociation rate constants on the different regions of the particle surface are modified. As a consequence of the induced change between the relative charges of the poles and the equator for each IPC, the overall particle charge is modified. Since a pH change is as fast as the H^+ ion diffusion and the ion diffusion is at least 2 orders of magnitude faster than the diffusion of isolated particles in the nanometer range, we are allowed to mimic the effect of a pH modification by suddenly changing the interaction parameters at a given MC step. It is worth noting that IPCs in the monomeric state between neutral walls diffuse one particle diameter in about 13000 MC steps, while in the self-assembled states the diffusive dynamics of the nanoparticles is much slower.

The ensuing changes in the system are quantified by recording some key properties as functions of time (i.e., MC cycles) along the charging−decharging−charging process, namely, the particle−wall energy (e_{cw}), the particle−particle energy (e_{cc}), and the order parameters Φ_4 and Φ_6, the latter ones being defined as[42]

$$\Phi_n = \left\langle \frac{1}{N}\sum_{i=1}^{N} \left| \left\langle \frac{1}{N_n}\sum_{j=1}^{N_n} \exp(in\theta_{ij}) \right\rangle \right| \right\rangle \quad (1)$$

where N is the total number of particles, N_n is the number of nearest neighbors of particle j, θ_{ij} is the angle between the ij-particle bond vector and an arbitrary direction in space, and $n = 4$ or 6. Data recorded along a full charging−decharging−charging cycle are shown in panels B1−B3 and C1−C3 of Figure 1 complemented by the corresponding characteristic

dx.doi.org/10.1021/nl500934v | Nano Lett. 2014, 14, 3412−3418

unit cell (insets in panels B1−B3) and by partial snapshots (insets in panels C1−C3).

For the case $Z_wZ_p < 0$ (panels B1 and C1 of Figure 1), the grain-like particle arrangement of the charged IPCs forms a well-defined layer which floats over the substrate, resulting into $e_{cw} \sim 0$. As the particles are decharged, the ordered structure immediately melts into a spatially disordered arrangement of isolated particles adsorbed on the substrate with their orientational vectors perpendicular to the confining wall. Both features as well as the surprising rapidity of this process are reflected in the accumulated key properties: (i) after decharging has set in, e_{cw} drops rapidly and eventually levels off to its equilibrium value of ~ -4.5, corresponding to the minimum of the particle−wall interaction; (ii) concomitantly, the particle−particle interaction increases at a comparably fast rate: while e_{cc} assumes typical values of ~ -1.6 in the grain-like arrangement, it quickly increases toward zero when IPCs are decharged, indicating that the particles have essentially ceased to interact with each other. This transformation in the spatial order is quantified via the order parameter Φ_6, which changes at the same time rate as the energies: while Φ_6 attains a value close to unity in the essentially perfect hexagonal arrangement within the grain-like pattern, it rapidly drops upon decharging to $\Phi_6 \sim 0.5$. Upon charging particles again, a process sets in that is essentially inverse to the previous one: e_{cw} literally jumps from a value of ~ -4 to ~ 0, indicating that the now charged particles immediately form a layer that floats above the substrate. Concomitantly, e_{cc} drops abruptly and then relaxes toward its equilibrium value at $e_{cc} \sim -1.6$. Thus, particles quickly rearrange in a layer with an internal 6-fold spatial arrangement which, however, requires some equilibration time to reach the characteristic grain-like orientational order. A final comparison of the energy values and of the order parameter data at the beginning and at the end of the cycle confirms that for $Z_wZ_p < 0$ the entire charging−decharging−charging process is fully reversible.

For the case of a neutral substrate (panels B2 and C2 of Figure 1), the particle−wall interaction is always zero, and the particles form—irrespective of their overall charge—triangular domains. During the decharging cycle a transformation from a grain- to a flower-like particle arrangement takes place, and the opposite process occurs at the same speed during the charging cycle. While the spatial structure remains invariant (reflected by the fact that Φ_6 attains, throughout, values close to unity), a substantial reorientation of the particles takes place: IPCs that form the circumference of a hexagonal tile have to undergo both vertical and horizontal redirections of their symmetry axes, while the orientation of the central particle has to be rotated by 90° into a direction pointing perpendicular to the confining wall. Still, the energetic costs for these reorientations are surprisingly small, reflected by the fact that in the immediate vicinity of the charge switch only small changes in e_{cc} occur. The subsequent, relatively moderate decay of e_{cc} as a function of time provides evidence that the reorientation of the particles is rather slow. The tiny overall decrease in e_{cc} at the end of the cycle might be related to the observation that the regions of uniform internal, ordered structure have grown in size along the whole process.

The most dramatic structural changes induced by the charging-decharging process are observed for the case $Z_wZ_p > 0$ (panels B3 and C3 of Figure 1). The decharging process transforms a grain-like particle arrangement with 6-fold coordination into a square lattice with 4-fold coordination, inducing thereby a significant spatial and orientational reordering. These rearrangements are realized while the particles keep their vertical positions strictly in a well-defined monolayer adsorbed on the substrate. During the transformation of grain-like configurations into square domains the induced, initial and moderate increase in e_{cc} levels off to a value that is slightly larger than the e_{cc}-value of the hexagonal equilibrium structure; concomitantly, the order parameter Φ_4 increases and saturates at a value close to ∼0.9, which is lower than the corresponding Φ_6-value for the preceding grain-like particle arrangement. This is due to the fact that while hexagonal domains can easily merge due to their symmetry, square-like domains may have non compatible mutual orientation. Charging the particles again leads, at the end of a slow equilibration process, to an e_{cc}-value which is close to but slightly larger than the corresponding value at the end of the first process segment; rather surprisingly, the order parameter Φ_6 saturates during this segment of the process already at a value close to ∼0.7, while Φ_4 tends within this time window toward ∼0.35. A closer, visual inspection of the corresponding particle configuration provides an explanation for this tendency: at the end of the entire cycle relatively large islands with internal square-like particle arrangements persist amidst regions with internal hexagonal, grain-like order. Energetic considerations (see Figure 2) demonstrate that the grain-like pattern is highly unstable for overall neutral IPCs, while square domains are energetically metastable for charged IPCs. Summarizing, for the case $Z_wZ_p > 0$, a continued application of charging−decharging cycles will eventually lead to a mixed state with regions of both hexagonal and square symmetry,

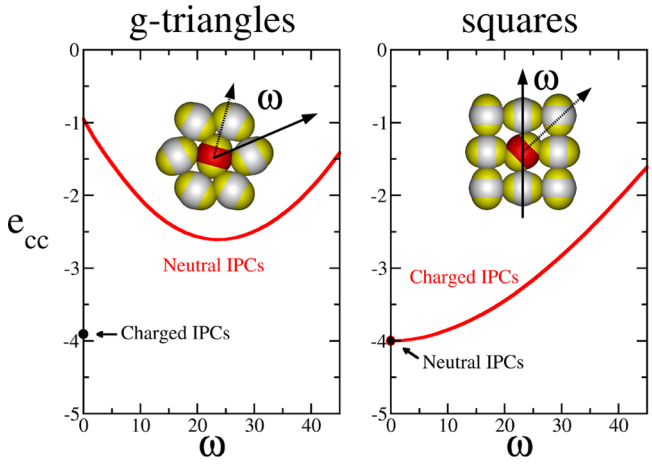

Figure 2. Analysis of the particle−particle energy, e_{cc}, for simplified, fully two-dimensional, isolated units of the microcrystalline domains observed when $Z_wZ_p > 0$. Left/right: Neutral/charged IPCs are forced to be arranged into a g-triangle/square configuration, and the energy of the central particle (colored in red) is reported as a function of small angular rotations of this particle (defined by the angle ω) with respect to the equilibrium orientation; in the snapshot, the continuous arrow indicates the equilibrium orientation ($\omega = 0°$), while the dotted arrow defines the angle ω. The corresponding internal energy of the central particle for neutral/charged IPCs in its equilibrium orientation in a g-triangle/square configuration is also reported for comparison. Note that in the grain-like patterns observed in the simulations the orientational vectors of two neighboring IPCs—in contrast to the idealized scenario considered here—are not fully horizontal, as shown in Figure 3 of the Supporting Information.

dx.doi.org/10.1021/nl500934v | Nano Lett. 2014, 14, 3412−3418

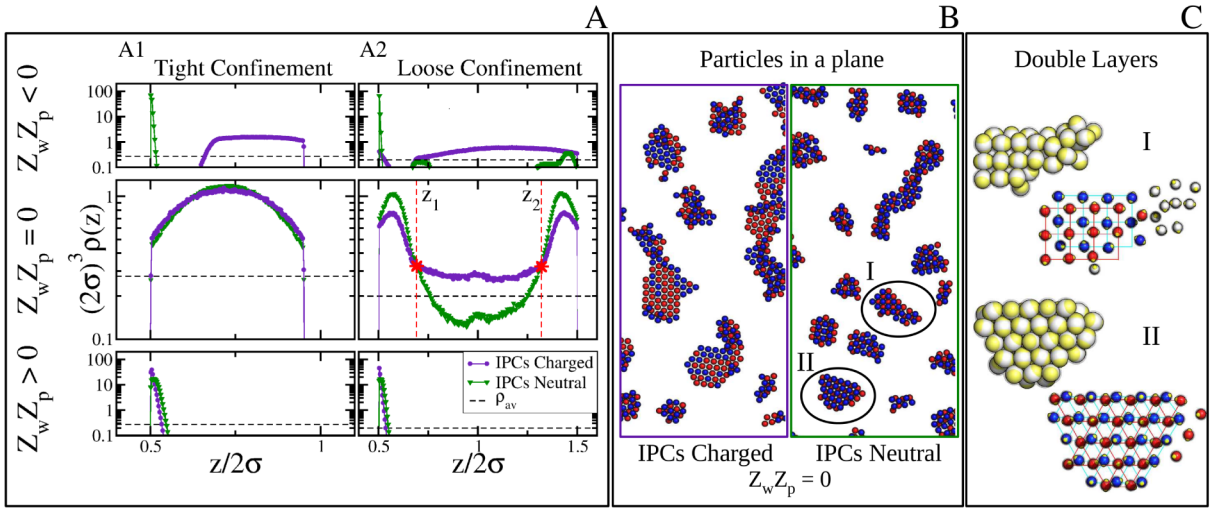

Figure 3. Panel A: density profiles $\rho(z)$ of the two investigated types of IPCs—i.e., overall charged and neutral particles, as labeled—under tight/loose (column A_1/A_2) confinement. In both columns, central panels refer to the case $Z_wZ_p = 0$, while top/bottom panels show the results for the cases $Z_wZ_p < 0$ and $Z_wZ_p > 0$, respectively. The black dashed line in all of these panels indicates the average number density ρ_{av}. The red asterisks in the central panel of column A2—and the corresponding vertical dashed lines—indicate the intersection points of the density profiles; the corresponding z-values of such intersections are labeled as z_1 and z_2. Panel B: slices of typical simulation snapshots in loose confinement are shown for charged/neutral particles (left/right inset); the color of a particle specifies its z-coordinate: red is used for particles with $z < 2\sigma$ (bottom layer), blue for particles with $z > 2\sigma$ (top layer). Inside the right inset of panel B, two clusters are highlighted and referred to as I and II. Panel C: magnified views of clusters I and II; on the left particles are drawn to scale (gray particles with yellow patches); on the right the particle size is reduced to improve visualization of the underlying lattice; in the latter case particles in the bottom layer are colored in red, while the particles in the top layer are colored in blue; lines between the centers of mass of the particles are traced out to highlight the lattice structure. In cluster I a few particles that are not ordered are shown in the original color.

meaning that the charging−decharging−charging process is not completely reversible.

If we consider overall neutral IPCs and suddenly switch the sign of the wall charge from the case $Z_wZ_p < 0$ to the case $Z_wZ_p > 0$, we observe a transition from a monomeric phase to a microcrystalline gel with square-like domains, a transformation which is fully reversible when the charge of the substrate is switched back to its original value, as shown in Figure 5 of the Supporting Information. Since the charge of the substrate can be externally controlled,[17] the self-assembly of the particles into a microcrystalline gel with square-like domains can be switched on and off in a fully reversible way.

The different assembly scenarios observed under tight confinement conditions show the tendency of IPCs to form quasi two-dimensional aggregates with a well-defined, internal structure that depends on the system parameters. The planarity of the aggregates is quantified by estimating the density profile, $\rho(z)$. Data are reported in panel A of Figure 3.

Under tight confinement conditions (column A1 of Figure 3), particles are not able to assemble along the z-direction; thus the density profiles of both neutral and charged IPCs between neutral walls (central panel of column A1 in Figure 3) are symmetric with respect to the center of the simulation box along the z-axis. In contrast, in most cases with $Z_wZ_p \neq 0$, IPCs tend to strongly adsorb to the bottom wall, meaning that the $\rho(z)$ at the bottom of the sample assumes extremely large values as compared to the rest of the system (top/bottom panels of column A1 in Figure 3). More specifically, when $Z_wZ_p \neq 0$, neutral particles fully adsorb to the substrate, forming either a disordered fluid-like phase (when $Z_wZ_p < 0$) or a microcrystalline gel with square-like domains (when $Z_wZ_p > 0$). Overall charged IPCs, on the other hand, behave differently depending on the wall charge. When $Z_wZ_p < 0$, a particle layer is formed, characterized by grain-like domains, which maximizes the distance to the substrate as a consequence of the repulsion between the charged bottom wall and the exposed equators of the particles within the crystalline domains; the resulting structure is a microscrystalline gel that floats over the bottom wall, i.e., $\rho(\sigma) \ll 1$. In contrast, when $Z_wZ_p > 0$, charged IPCs self-organize into a grain-like gel which is fully adsorbed on the substrate. As mentioned above, due to the reduced particle mobility, the microcrystalline gel, though retaining the characteristic spatial and orientational order of charged IPCs assemblies, is formed by domains smaller than those constituting the other grain-like structures.

A final question to be addressed concerns how the described self-assembly scenarios change when the confinement is slightly released. Under loose confinement conditions (column A2 of Figure 3), particles are allowed to aggregate also along the vertical direction. The density profiles reveal that, when the bottom wall is charged, electrostatics dominates over the geometric confinement, meaning that both neutral and charged particles behave similar to the corresponding tight confinement cases (top/bottom panels of column A2 in Figure 3). A visual inspection of the particle configurations reveals that, when $Z_wZ_p \neq 0$, the self-assembly scenarios of both neutral and charged IPCs are completely unaffected by the change in confinement, meaning that depending on the control parameters we observe again a fluid-like phase and grain-like/square-like particle networks. In contrast, when the bottom wall is neutral, particles assemble into both mono- and bilayers, irrespective of their overall charge (central panel of column A2 in Figure 3).

A more profound analysis of the single- and double-layered aggregates formed by IPCs between neutral walls reveals a quite rich scenario according to the particle charge. We quantify the percentage of particles in a monolayers via

dx.doi.org/10.1021/nl500934v | Nano Lett. 2014, 14, 3412−3418

$$N_p/N = \frac{L^2}{N}\int_{z_1}^{z_2} \rho(z)\, dz \quad (2)$$

where N is the total number of particles in the simulation box, L is the lateral size of the box along the x- and y-directions, and $z_{1,2}$ are suitable boundaries for the vertical coordinates of the particles that belong to a monolayer. To have the same boundaries for neutral as well as charged particles, $z_{1,2}$ are defined as the intersection points between the density profiles $\rho(z)$ of the two different particle charges: the configurations leading to the peaks at $z < z_1$ or $z > z_2$ are typically double-layered structures, whereas those that bring forward the nonvanishing $\rho(z)$-values for $z_1 \leq z \leq z_2$ are predominantly monolayers. We find that $N_p/N \approx 0.28$ for neutral IPCs, while $N_p/N \approx 0.45$ for charged IPCs. Hence, overall neutral particles tend to form double-layered aggregates, whereas overall charged particles assemble into double- or single-layers with equal probability.

The quantitative information provided by N_p/N is also supported by the snapshots displayed in panel B of Figure 3 that reproduces significant portions of the two systems where particles in the lower or upper part of the box are distinguished by their color. A further analysis of the system configurations reveals that, while monolayers of charged particles retain the characteristic grain-like structure, the corresponding double-layered aggregates do not have a well-defined internal order, suggesting that deviations from planar, grain-like assemblies are likely due to the deep quench in temperature experienced by the system. In contrast, double-layered structures formed by neutral particles do have an internal order.

Magnified views of two characteristic double-layered clusters of neutral IPCs between neutral walls are shown in panel C of Figure 3 to better visualize their structure. Surprisingly, both the spatial and the orientational order of the particles differ significantly in the two selected cases: cluster I is mainly composed by two superimposed square lattices where particles have a T-shaped reciprocal orientation within each layer, while cluster II consists of two, noncentered, triangular layers where particles assume the characteristic flower-like pattern observed for neutral IPCs close to a neutral substrate. A careful inspection of other clusters and other configurations confirms that most of the neutral particles are assembled into these two types of double layers. Such a phenomenon is likely due to the competition between the square-like and the flower-like particle arrangements. We can thus conclude that under loose confinement between neutral walls both neutral and charged IPCs form nonplanar aggregates, but as soon as the substrate is weakly charged IPCs typically assemble into monolayers whose internal, spatial and orientational morphology can be externally tuned.

In summary, we have investigated the self-organization of heterogeneously charged particles on a substrate of variable charge. We have shown that, due to the complex interplay between the highly directional particle−particle and particle−wall interactions, it is possible to externally control (i) the occurrence of self-assembly (extended clusters forming a microcrystalline gel versus isolated monomers), (ii) the internal spatial order of the emerging crystalline domains constituting the branches of the gel networks (square-like versus triangle-like domains), and (iii) the bonding patterns of such aggregates (grain-like versus flower-like particle arrangements). Using the pH, the salinity, and the wall charge as external control parameters, one self-assembly scenario can be transformed into another in a reversible fashion. Even though the selected IPC systems have been investigated following a deep quench, additional simulations reveal that the morphology of the discussed self-assembly scenarios is maintained for less deep quenches or annealing processes, whereas the cluster size distribution is of course temperature-dependent.

The tendency of IPCs to self-assemble into quasi two-dimensional aggregates has been observed in most of the investigated cases. Double-layered aggregates were found only for IPCs between neutral walls in a loose confinement geometry. As soon as the substrate is (even weakly) charged, adsorption wins over confinement, and it becomes possible to control the assembly of essentially planar aggregates, their size, and their internal structure independently of the confinement. The adsorbed microcrystalline gels can be composed of aggregates of different typical size due to the competition between optimizing the particle−particle bonding and the adsorption to the substrate. Grain-like domains adsorbed to the bottom wall are indeed smaller than adsorbed square-like domains; the reason for this feature is likely related to the compatibility between the perfect planar orientation of IPCs in square domains as compared to the slightly out of plane orientations between nearest neighbors within a grain-like domain. Finally, in systems forming double-layered aggregates, the competition between attractive and repulsive directional interactions is most likely responsible for the different forms of colloidal ordering within double-layered structures.

■ ASSOCIATED CONTENT

Supporting Information

Additional information and figures. This material is available free of charge via the Internet at http://pubs.acs.org.

■ AUTHOR INFORMATION

Corresponding Author

*E-mail: emanuela.bianchi@tuwien.ac.at.

Notes

The authors declare no competing financial interest.

■ ACKNOWLEDGMENTS

The authors thank Peter van Oostrum for fruitful discussions. E.B. thanks Moritz Antlanger for technical support. Financial support by the Austrian Science Foundation (FWF) under project nos. M1170-N16, V249-N27, P23910-N16, and F41 (SFB ViCoM) is gratefully acknowledged.

■ REFERENCES

(1) Shipway, A. N.; Katz, E.; Willner, I. Nanoparticle Arrays on Surfaces for Electronic, Optical, and Sensor Applications. *ChemPhysChem* **2000**, *1*, 18−52.

(2) Velev, O. D.; Kaler, E. W. In Situ Assembly of Colloidal Particles into Miniaturized Biosensors. *Langmuir* **1999**, *15*, 3693−3698.

(3) Vogel, N.; Weiss, C. K.; Landfester, K. From soft to hard: the generation of functional and complex colloidal monolayers for nanolithography. *Soft Matter* **2012**, *8*, 4044−4061.

(4) Vogel, N.; Belisle, R. A.; Hatton, B.; Wong, T.-S.; Aizenberg, J. Transparency and damage tolerance of patternable omniphobic lubricated surfaces based on inverse colloidal monolayers. *Nat. Commun.* **2012**, *4*, 2177.

(5) Barth, J. V.; Costantini, G.; Kern, K. Engineering atomic and molecular nanostructures at surfaces. *Nature* **2005**, *437*, 671−679.

(6) Schlickum, U.; Decker, R.; Klappenberger, F.; Zoppellaro, G.; Klyatskaya, S.; Ruben, M.; Silanes, I.; Arnau, A.; Kern, K.; Brune, H.;

et al. Metal-Organic Honeycomb Nanomeshes with Tunable Cavity Size. *Nano Lett.* **2007**, *7*, 3813−3817.
(7) Blunt, M. O.; Russell, J. C.; Gimenez-Lopez, M. d.; Garrahan, J. P.; Lin, X.; Schröder, M.; Champness, N. R.; Beton, P. H. Random Tiling and Topological Defects in a Two-Dimensional Molecular Network. *Science* **2008**, *322*, 1077−1081.
(8) Kim, S.-H.; Lee, S. Y.; Yang, S.-M.; Yi, G.-R. Self-assembled colloidal structures for photonics. *NPG Asia Mater.* **2011**, *3*, 25−33.
(9) Russel, W. B.; Saville, D. A.; Schowalter, W. R. *Colloidal Dispersions*; Cambridge University Press: Cambridge, U.K., 1995.
(10) Li, F.; Josephson, D. P.; Stein, A. Colloidal assembly: the road from particles to colloidal molecules and crystals. *Angew. Chem., Int. Ed.* **2011**, *50*, 360−388.
(11) Law, A. D.; Buzza, D.; Horozov, T. S. Two-dimensional colloidal alloys. *Phys. Rev. Lett.* **2011**, *106*, 128302.
(12) Law, A. D.; Auriol, M.; Smith, D.; Horozov, T. S.; Buzza, D. Self-assembly of two-dimensional colloidal clusters by tuning the hydrophobicity, composition, and packing geometry. *Phys. Rev. Lett.* **2013**, *110*, 138301.
(13) Osterman, N.; Poberaj, I.; Dobnikar, J.; Frenkel, D.; Ziherl, P.; Babič, D. Field-Induced Self-Assembly of Suspended Colloidal Membranes. *Phys. Rev. Lett.* **2009**, *103*, 228301.
(14) Weddemann, A.; Wittbracht, F.; Eickenberg, B.; Hütten, A. Magnetic Field Induced Assembly of Highly Ordered Two-Dimensional Particle Arrays. *Langmuir* **2010**, *26*, 19225−19229.
(15) Leunissen, M. E.; Vutukuri, H. R.; van Blaaderen, A. Directing colloidal self-assembly with biaxial electric fields. *Adv. Mater.* **2009**, *21*, 3116−3120.
(16) Tierno, P.; Fischer, T. M.; Johansen, T. H.; Sagués, F. Colloidal assembly on magnetically vibrated stripes. *Phys. Rev. Lett.* **2008**, *100*, 148304.
(17) Ristenpart, W. D.; Aksay, I. A.; Saville, D. A. Electrically guided assembly of planar superlattices in binary colloidal suspensions. *Phys. Rev. Lett.* **2003**, *90*, 128303.
(18) Khalil, K. S.; Sagastegui, A.; Li, Y.; Tahir, M. A.; Socolar, J. E. S.; Wiley, B. J.; Yellen, B. B. Binary colloidal structures assembled through Ising interactions. *Nat. Commun.* **2012**, *3*, 794.
(19) Nych, A.; Ognysta, U.; Škarabot, M.; Ravnik, M.; Žumer, S.; Muševič, I. Assembly and control of 3D nematic dipolar colloidal crystals. *Nat. Commun.* **2013**, *4*, 1489.
(20) Mangold, K.; Leiderer, P.; Bechinger, C. Phase Transitions of Colloidal Monolayers in Periodic Pinning Arrays. *Phys. Rev. Lett.* **2003**, *90*, 158302.
(21) Mikhael, J.; Roth, J.; Helden, L.; Bechinger, C. Archimedean-like tiling on decagonal quasi-crystalline surfaces. *Nature* **2008**, *454*, 501−504.
(22) Demirörs, A. F.; Pillai, P. P.; Kowalczyk, B.; Grzybowski, B. A. Colloidal assembly directed by virtual magnetic moulds. *Nature* **2013**, *503*, 99−103.
(23) van Blaaderen, A.; Ruel, R.; Wiltzius, P. Template-directed colloidal crystallization. *Nature* **1997**, *385*, 321−324.
(24) Rossi, L.; Sacanna, S.; Irvine, W. T. M.; Chaikin, P. M.; Pineb, D. J.; Philipse, A. P. Cubic crystals from cubic colloids. *Soft Matter* **2011**, *7*, 4139−4142.
(25) Barry, E.; Dogic, Z. Entropy driven self-assembly of non-amphiphilic colloidal membranes. *Proc. Natl. Acad. Sci. U.S.A.* **2010**, *8*, 10348−10353.
(26) Qi, W.; de Graaf, J.; Qiao, F.; Marras, S.; Manna, L.; Dijkstra, M. Ordered Two-Dimensional Superstructures of Colloidal Octapod-Shaped Nanocrystals on Flat Substrates. *Nano Lett.* **2012**, *12*, 5299−5303.
(27) Pawar, A. B.; Kretzschmar, I. Fabrication, Assembly, and Application of Patchy Particles. *Macromol. Rapid Commun.* **2010**, *31*, 150−168.
(28) Bianchi, E.; Blaak, R.; Likos, C. N. Patchy colloids: state of the art and perspectives. *Phys. Chem. Chem. Phys.* **2011**, *13*, 6397−6410.
(29) Chen, Q.; Bae, S. C.; Granick, S. Directed self-assembly of a colloidal Kagome lattice. *Nature* **2011**, *469*, 381−384.
(30) Gangwal, S.; Cayre, O. J.; Velev, O. D. Dielectrophoretic Assembly of Metallodielectric Janus Particles in AC Electric Fields. *Langmuir* **2008**, *24*, 13312−13320.
(31) Gangwal, S.; Cayre, O. J.; Bazant, M. Z.; Velev, O. D. Induced-Charge Electrophoresis of Metallodielectric Particles. *Phys. Rev. Lett.* **2008**, *100*, 058302.
(32) Smoukov, S. K.; Gangwal, S.; Marquez, M.; Velev, O. D. Reconfigurable responsive structures assembled from magnetic Janus particles. *Soft Matter* **2009**, *5*, 1285−1292.
(33) Gangwal, S.; Pawar, A.; Kretzschmar, I.; Velev, O. D. Programmed assembly of metallodielectric patchy particles in external AC electric fields. *Soft Matter* **2010**, *6*, 1413−1418.
(34) Kretzschmar, I.; Song, J. H. Surface-anisotropic spherical colloids in geometric and field confinement. *Curr. Opin. Colloid Interface Sci.* **2011**, *16*, 84−95.
(35) Bianchi, E.; Kahl, G.; Likos, C. N. Inverse patchy colloids: from microscopic description to mesoscopic coarse-graining. *Soft Matter* **2011**, *7*, 8313−8323.
(36) Bianchi, E.; Likos, C. N.; Kahl, G. Self-assembly of heterogeneously charged particles under confinement. *ACS Nano* **2013**, *7*, 4657−4667.
(37) Yang, J.; Elim, H. I.; Zhang, Q.; Lee, J. Y.; Ji, W. Rational synthsis, self-assembly, and optical porperties of PbS-Au heterogeneous nanostructures via preferential deposition. *J. Am. Chem. Soc.* **2006**, *128*, 11921−11926.
(38) Christian, D. A.; Tian, A.; Ellenbroek, W. G.; Levental, I.; Rajagopal, K.; Janmey, P. A.; Liu, A. J.; Baumgart, T.; Discher, D. E. Spotted vesicles, striped micelles and Janus assemblies induced by ligand binding. *Nat. Mater.* **2009**, *8*, 843−849.
(39) Daniel, M.-C.; Tsvetkova, I. B.; Quinkert, Z. T.; Murali, A.; De, M.; Rotello, V. M.; Cheng Kao, C.; Dragnea, B. Role of surface charge density in nanoparticle-templated assembly of Bromvirus protein cages. *ACS Nano* **2010**, *4*, 3853−3860.
(40) Božič, A. L.; Podgornik, R. Symmetry effects in electrostatic interactions between two arbitrarily charged spherical shells in the Debye-Hückel approximation. *J. Chem. Phys.* **2013**, *138*, 074902.
(41) Liu, Z.; Qiao, J.; Niu, Z.; Wang, W. Natural supramolecular building blocks: from virus coat proteins to viral nanoparticles. *Chem. Soc. Rev.* **2012**, *41*, 6178−6194.
(42) Steinhardt, P. J.; Nelson, D. R.; Ronchetti, M. Bond-orientational order in liquids and glasses. *Phys. Rev. B* **1983**, *28*, 784−805.